The Journal of Chemical Physics

RESEARCH ARTICLE | JULY 17 2023

Dynamic structure factors of polymer melts as observed by neutron spin echo: Direct comparison and reevaluation

Michael Monkenbusch ; Margarita Kruteva ; Dieter Richter

J. Chem. Phys. 159, 034902 (2023)
https://doi.org/10.1063/5.0150811

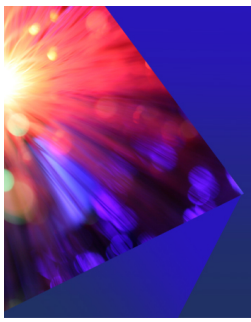

The Journal of Chemical Physics ARTICLE pubs.aip.org/aip/jcp

Dynamic structure factors of polymer melts as observed by neutron spin echo: Direct comparison and reevaluation

Cite as: J. Chem. Phys. 159, 034902 (2023); doi: 10.1063/5.0150811
Submitted: 16 March 2023 • Accepted: 26 June 2023 •
Published Online: 17 July 2023

Michael Monkenbusch,[1,a)] Margarita Kruteva,[1] and Dieter Richter[2]

AFFILIATIONS

[1] Forschungszentrum Jülich GmbH, Jülich Centre for Neutron Science (JCNS-1), 52425 Jülich, Germany
[2] Forschungszentrum Jülich GmbH, Jülich Centre for Neutron Science (JCNS-2), 52425 Jülich, Germany

[a)] **Author to whom correspondence should be addressed:** m.monkenbusch@fz-juelich.de

ABSTRACT

In this work, we compare the single chain dynamic structure factors for five different polymers: polyolefins (PE and PEP), poly-dienes (PB and PI), and a polyether (PEO). For this purpose, we have extended the De Gennes approximation for the dynamic structure factor. We describe the single chain dynamic structure factor in multiplying the coherent scattering functions for local reptation and Rouse motion within the Rouse blob. Important results are (i) the simple De Gennes structure factor $S(Q,t)_{\mathrm{DG}}$ approximates within a few Å the outcome for the tube diameter of the more elaborate structure factor (exception PI); (ii) the extended De Gennes structure factor together with the Rouse blob describes the neutron spin echo spectra from the different polymers over the complete momentum transfer range and the full time regime from early Rouse motion to local reptation; and (iii) the representation of the scattering functions could significantly be improved by introducing non-Gaussianity corrections to the Rouse-blob dynamics. (iv) The microscopic tube step length in all cases is significantly larger than the rheological one; further tweaking the relation between tube length and entanglement blob size may indicate a possible trend toward an anisotropic lean tube with a step-length larger than the lateral extension. (v) All considered polymer data coincide after proper (Q,t) scaling to a universal behavior according to the length scale of the tube, while the relevant time scale is the entanglement time τ_e. (vi) In terms of the packing model, the required number of chains spanning the entanglement volume consistently is about 40% larger than that obtained from rheology.

I. INTRODUCTION

High molecular weight polymer melts and solutions exhibit unique rheological properties such as viscoelasticity with rubber-like behavior at intermediate times and very long terminal relaxation times accompanied by high viscosities, shear thinning, strain hardening, and hierarchical relaxation of branched polymers. They originate from topological constraints that are imposed by the mutually interpenetrating chains. These constraints or entanglements lead to preferred motion in the direction of the chain contour. Much progress in the understanding of polymer chain dynamics was achieved in terms of tube models based on the reptation mechanism.[1–9] The reptation model describes the resulting topological constraints through a virtual tube that follows the primitive path of a given test chain. Chains slither along this tube, thereby obeying the topological constraints. The tube is characterized by its "diameter" d, which is also taken as its step-length, and by its contour length L. Refinements addressing contour length fluctuations (CLFs) of a chain in its tube, as well as the effect of constraint release (CR), represent the state of the art.[5] The dynamics of short linear chains or the dynamics of long entangled chains at short times within the tube is commonly described in terms of the Rouse model.[10] There, the chains are considered to move independently in the heat bath created by the surrounding chains. Entropic restoring forces counterbalance the heat bath related frictional forces that manifest themselves locally on the monomer level.

Aside from the phenomenological reptation approach, theoretical concepts were brought forward, aiming for an understanding of the dynamics in long chain melts on a more fundamental level. In the mode coupling theory (MCT) approach of Schweizer,[11–17] the tube

ideas are replaced by strong nonlinear couplings between collective density fluctuations on the scale of the chain radius of gyration R_g. Guenza considered a generalized Langevin equation (GLE), where, as a result of chain interpenetration, the chain motion is coupled within the range of their radius of gyration by a Gaussian interchain potential of mean force.[18–20] Recently, Guenza hypothesized that, in strongly entangled melts, cooperative chain fluctuations are restricted to the entanglement volume d^3.[21]

With the increasing sophistication of high resolution neutron spin echo (NSE) spectroscopy,[23,24] the length and time scales allow access to the chain dynamics under tube constraints.[25–29] It is interesting to note that parallel to the progress in neutron scattering instrumentation, the capabilities of simulations reached similar levels in space time exploration,[6,30] and both techniques began to complement each other.

With a few exceptions,[31,32] nearly all NSE investigations addressed the single chain dynamic structure factor that is obtained from experiments on systems where a few labeled (hydrogenated) chains are immersed in a deuterated matrix of the same polymer. Under these contrast conditions, the experiment observes coherent scattering from the ensemble of monomers making up the labeled chain. In this work, we name this quantity "dynamic structure factor" $S(Q,t)$, omitting the "single chain," while incoherent scattering as obtained from a hydrogenous melt directly leads to the monomer mean squared displacement, the interpretation of the coherent scattering that relates to the single chain pair correlation function is more demanding. In 1981, De Gennes[33] proposed an analytic first order approximation for $S(Q,t)$

$$S(Q,t) = 1 - \frac{Q^2d^2}{36} + \frac{Q^2d^2}{36}\exp\left(\frac{u^2}{36}\right)\mathrm{erfc}\left(\frac{u}{6}\right), \tag{1}$$

where $u^2 = t/\tau_0$, with τ_0 setting the time scale. Later on, Eq. (1) has been used in its exponentiated form [Eq. (2)][27] not only to interpret basically all further NSE experiments on polymer melts but also simulation results[7] (and references therein[6,34–38]). These experiments were able to manifest the existence of an intermediate length for polymer dynamics and provided a microscopic proof of a well-defined length scale for the topological constraints.

In general, the simple approach [Eq. (1)] fails to describe the scattering function at short times. Also, the experimental data in that short time regime are rather close to a stretched exponential with a stretching exponent of about 1/2 and, thus, strongly deviating from 0.83, which approximates[39] the Rouse intermediate scattering function. Coarse grained MD simulations have been used to shed light on the reptation scenario.[6,7] Using a "slip-link" model, Likthman[8] could reproduce the then available $S(Q,t)$ data of PE and PEB over the full time range and reproduce rheology data by adjusting friction, Kuhn length, and slip-link parameters: density, length, and friction.

Furthermore, very recently, we performed NSE on the motion of short tracer chains in highly entangled melts.[40] Unexpectedly, the tracers were found to undergo sub-diffusion over a distance very close to the tube diameter of the respective highly entangled host. The cross-over distance to Fickian diffusion is, thereby, independent of the tracer's length. Beyond this cross-over distance, the Fickian diffusivity agreed with the macroscopic results. In addition, we found that the Rouse dynamics of the tracers is strongly non-Gaussian (NG), with a related segment displacement distribution narrower than the Gaussian counterpart. These results were understood as a consequence of the highly cooperative motion of the tracers with the host, mirroring the host dynamics within the host matrix.

Thus, a comprehensive description of $S(Q,t)$ from first principles but also from simpler modeling assumptions, which allows straightforward and easy to use assessment of $S(Q,t)$ data from scattering experiments, is still missing.

Here we discuss a semi-empirical approach to achieve the latter by extensions based around De Gennes' initial approach. These were guided by the experimentally observed properties of $S(Q,t)$ considered in light of the general understanding of the reptation scenario. Thus, the approach is rather an extension to scrutinize, i.e., extract information of the observable geometry and motion properties supplied by the experimental observations, i.e., the $S(Q,t)$ from NSE, than an attempt to derive it from first principles. It provides readily extractable space and time scales of the reptation scenario for a certain polymer under observation. Such an approach yields an important practical tool for classification, interpolation, and "analytic" description of the full scattering functions of entangled polymer systems in terms of a few parameters. Namely, these are (i) the entanglement length scale, (ii) the dynamical timescale (Rouse rate), and eventually (iii) in order to address residual small deviations at large Q and intermediate time t—the amplitude of non-Gaussianity effects. The role of tentative decoupling of entanglement length and "blob" size has further been explored.

Extending the De Gennes concept for local reptation, here we reanalyze NSE data on five different polymers: polyolefins, polydienes, and a polyether. In Secs. II and III, we present the theoretical context, and then in Sec. IV, we present the experiments and the data evaluation. In Sec. V, we discuss the outcome of the various fits and interpret the results. Then in Sec. VI, we discuss the presented expressions ability to accurately reproduce $S(Q,t)$ of reptating polymers, addressing the aspect of how, independent of physical parameter assignments, the presented approaches may serve as technical interpolation tools. Finally, in Sec. VII, we critically discuss the results and summarize the main results.

II. THEORETICAL CONSIDERATIONS

A. De Gennes approximation for the dynamic structure factor

So far, the evaluation of NSE data on various polymers was based on the approximated De Gennes' description of local reptation of the following form:

$$\frac{S_{\mathrm{DG}}(Q,t)}{S(Q)} = \left(1 - \exp\left[-\frac{Q^2d^2}{36}\right]\right) + S^{\mathrm{loc}}(Q,t)\exp\left[-\frac{Q^2d^2}{36}\right]S^{\mathrm{creep}}(Q,t), \tag{2}$$

with $S^{\mathrm{loc}}(Q,t) = \exp(t/\tau_0)\,\mathrm{erfc}\left(\sqrt{t/\tau_0}\right)$ and $\tau_0 = 36/(Wl^4Q^4)$. Where d is the tube diameter, Wl^4 is the so called Rouse rate that relates to the monomeric friction coefficient ξ by $Wl^4 = 3k_BTl^2/\xi$, and Q is the momentum transfer during scattering. In the Rouse

model, Wl^4 is scale invariant; here we use $l = l_{seg} = \sqrt{C_\infty l_0^2 n_b}$ with n_b being the number of bonds of length l_0 per monomer and C_∞ being the characteristic ratio. Considering the NSE time window of at maximum 1000 ns, for all practical purposes, $S^{creep}(Q,t) = 1$. For long chains, Eq. (1) is an approximation of De Gennes' result[33] [see Eq. (3.12) in Ref. 33] toward a larger Q, assuming that his expression is the first term of a Taylor expansion of $\exp\left[-Q^2d^2/36\right] \cong 1 - Q^2d^2/36 + O(Q^4)$, and $S^{creep}(Q,t) = 1$. Inserting this expansion in Eq. (2), De Gennes' original expression [Eq. (1)] reemerges as follows:

$$\frac{S_{DG}(Q,t)}{S(Q)} \cong \left[\left(1 - \frac{Q^2d^2}{36}\right) + \frac{Q^2d^2}{36} S^{loc}(Q,t)\right] + O(Q^4), \quad (3)$$

with $d = l_{seg}\sqrt{N_e}$, and N_e being the length of an entanglement strand. The problem with this simple approach is its incompleteness and the missing Rouse relaxation that determines the scattering function at shorter times $t \le \tau_e$, where τ_e is the entanglement time,

$$\tau_e = \frac{d^4}{\pi^2 W l^4}. \quad (4)$$

In order to distinguish results for the tube diameter obtained by fitting with Eq. (2) from other approaches, we name the, thus, determined value d_{DG}.

B. The role of contour length fluctuations

For completeness of the discussions, we mention that, with the exception of polybutadiene with a molecular weight of (M_w) 45 kg/mol (PB45), all investigated polymer melts are very highly entangled, such that contour length fluctuations (CLFs) do only marginally contribute within the observation window of NSE. This is not the case for the PB45-melt: With $N/N_e = Z = 17$, the CLF processes contribute to $S(Q,t)$ within the observation range of NSE. The fluctuating chain ends lead to an apparently wider tube than what would be observed for a higher M_w.[41,42] Based on Clarke and Mcleish,[43] Wischnewski *et al.*[42] have presented an explicit dynamic structure factor for polymers undergoing reptation and CLF

$$S^{CLF}(Q,t) = \frac{N}{2\mu^2}\left[2\mu + e^{-2\mu} + 2 - 4\mu\, s(t) - 4e^{-2\mu s(t)} + e^{-4\mu s(t)}\right], \quad (5)$$

with $\mu = Q^2 l_{seg}^2/12$ and $s(t) = (1.5/Z)\,(t/\tau_e)^{\frac{1}{4}}$. $s(t)$ describes the time dependent release of segments (monomers) from the tube by CLF. $S^{CLF}(Q,t)$ corresponds to $S^{creep}(Q,t)$ in Eq. (2).

III. MODEL COMBINING ROUSE-BLOB DYNAMICS AND LOCAL REPTATION

In order to achieve a more complete description of a chain undergoing local reptation, we undertook the following three steps:

(i) We carried out the full integration of the local reptation structure factor mentioned in Eq. (3.11) in (De Gennes[33]) and
(ii) calculated the Rouse dynamic structure factor of an entanglement blob.
(iii) We combined the scattering function of the coarse grained chain (to the tube step length) with local reptation multiplied with the proper fluctuation amplitude and with the Rouse-blob contribution.

Fully evaluating the De Gennes local reptation structure factor from Ref. 33 yields

$$S_{locrep} = \int_0^L \int_0^L \Sigma(s_1 - s_2, t) \exp\left[-\frac{Q^2 l_{seg}}{6\,u}|s_1 - s_2|\right] ds_1\, ds_2, \quad (6)$$

with contour length $L \simeq N/N_e \times d_{tube}$ (N = the number of monomers in the chain) and an average "stretch" per segment $u = l_{seg}/\sqrt{N_e}$. The density fluctuation along the tube contour is called "local reptation" and has the shape of a diffusing 1D density fluctuation along the contorted tube (described by the coordinate s)

$$\Sigma(s,t) = A + \frac{B}{\sqrt{4\pi\Delta t}} \exp\left(-\frac{s^2}{4\Delta t}\right), \quad (7)$$

with the average line density $A = (N_e/d_{tube})^2$ and a fluctuation amplitude B and $\Delta = W l_{seg}^2/N_e$; s is a coordinate along the chain of contour L.[33]

Exactly following De Gennes exposition in Ref. 33 and inserting the proper scales, and integrating Eq. (6) yields an elastic part of Eq. (6) that has the form of a Debye function

$$S_{Debye}(Q) = \frac{72N}{N^2 l_{seg}^4 Q^4}\left[\exp\left(-\frac{l_{seg}^2 Q^2 N}{6}\right) + \frac{l_{seg}^2 Q^2 N}{6} - 1\right]. \quad (8)$$

We note, however, that in its coarse grained form, it has to level off at a Q corresponding to the blob size; the level pertains to the average blob size (see the supplementary material); and this is an important aspect of our reformulation in Eq. (10).

Inserting Eq. (7) into (6) and performing the time dependent integral representing the "local reptation fluctuations" reveals

$$\begin{aligned} S_{locrep}(Q,t) = {} & \frac{2N_e}{3}\sqrt{\frac{Wt}{\pi}}\left[\exp\left(-\frac{l_{seg}^2 Q^2 N}{6} - \frac{N^2}{4Wt}\right) - 1\right] \\ & + N_e\left[\frac{N}{3} + \frac{l_{seg}^2 Q^2 Wt}{9}\right]\exp\left(\frac{l_{seg}^4 Q^4 Wt}{36}\right) \\ & \times\left\{\mathrm{erfc}\left(\frac{l_{seg}^2 Q^2\sqrt{Wt}}{6}\right) - \mathrm{erfc}\left(\frac{3N + l_{seg}^2 Q^2 Wt}{6\sqrt{Wt}}\right)\right\}. \end{aligned} \quad (9)$$

This derivation has the drawback that it does not explicitly take into account the lateral extension and the internal Rouse dynamics of the entanglement "blobs."

In addition, it violates the condition that a long chain should exhibit the structure factor $S(Q, t = 0)$ of a Gaussian chain. In Ref. 33, this is addressed by a correction factor, and further, it is already noted that the integral treatment of Eq. (6) is valid only up to the length scale of the tube. In the here presented model, it is consistently taken into account in Eq. (10) by considering the effects of coarse graining (see the supplementary material) on the formu-

lation of the scattering function in combination with the scattering function of the entanglement "blobs."

A. Modeling additions

In order to address the above problem we revisit the model in order to get an approximation that allows us to deal with the local reptation fluctuation term and the Rouse blob inclusion in a consistent fashion.

Starting with $S(Q)$ of a Gaussian or freely joint (long) chain, we observe that this may (approximately) be described by a coarse grained chain with a step length corresponding to the alleged tube d_{tube} supplying scattering centers, each of which has an effective form-factor of the "blob." For equal scattering lengths of the "blob"-centers, the finite summation of the coarse grained chain would level at a larger Q at a constant $S(Q=0)/(N/Ne)$ instead of following the continuing $1/Q^2$-decay of the Debye function. Accounting for fluctuations in blob-scattering due to different numbers of segments realizing each tube-step at any given time, the large Q level is about 41% larger, as has been verified with inspection of simple random walks obtained by executing some basic MC inspection of walks with a constant and Gaussian distributed step length, see Fig. 1 and the supplementary material. Inspecting the variation of the number of chain-segments within each coarse grained tube step reveals a considerable variation around the average number N_e. This variation is a momentary instance of the density fluctuations that pertain to the amplitude B in Eq. (7). For random coarse grained chains, the simple Monte-Carlo scattering computations reveal that the "static" large Q-plateau and the fluctuation related constant large Q-values have a ratio of 1:2 to 1:3 [see the supplementary material for the illustration of the quality of the approximation assumptions entering Eq. (10)]. The quantitative analysis of simple MC results over a range of chain lengths step lengths and for Gaussian or freely joint chains yields a stable ratio of $\Xi \simeq 0.41$ between fluctuation and static contributions; as illustrated in Fig. 1 in the plateau region a constant ratio $C_w = (1+\Xi)C$ is encountered ($\Xi \simeq 0.41$), the Ξ value stays virtually the same for a broad range of random chain and step length parameters. This was used as a fixed ratio for the parameters from Eq. (6).

We note that in order to compare A and B from De Gennes' Ref. 33 in Eq. (7), a reference length is needed to make the ratio B/A dimensionless. Assuming the coarse graining length d_{tube} as reference and inserting De Gennes' expressions yields $B/(Ad) = 1/3$, close to but slightly less than the $\Xi = 0.41$ from the MC estimates.

Multiplying the resulting function with the form factor (scattering function) of the "blob" then yields a reasonable approximation to the full Debye structure function of the long chain, reestablishing the $1/Q^2$ behavior at a larger Q.

Thus, for the dynamic structure factor, the tube chain is modeled as

$$S_{\text{tube}}(Q,t) = \Big(S_{\text{Debye}}(Q)/N + N_e/N \times \Big[1+\Xi\Big\{\frac{3}{N N_e} S_{\text{locrep}}(Q,t)\Big\}\Big]\Big) \Big/ [1+(1+\Xi)\,N_e/N]. \tag{10}$$

Equations (9) and (8) each are scaled to 1 by $S_{\text{Debye}}(Q=0)/N = 1$, respectively, $\frac{3}{N N_e} S_{\text{locrep}}(Q, t=0) = 1$; the small forward intensity correction $1/[1+(1+\Xi)N_e/N]$ has no influence on the final normalized NSE curves representing $S(Q,t)/S(Q,t=0)$.

Finally, the full scattering function is approximated by multiplying it by the scattering function (in the sense of a form factor) of the (average) blob, as is further elaborated below in Sec. III B.

Equation (10), i.e., the local reptation part of the dynamic structure factor, depends on the total number of monomers N, the length of an entanglement strand N_e, implying a tube size $d = l_{\text{seg}}\sqrt{N_e}$ and on a rate parameter $W = (Wl^4)/l_{\text{seg}}^4$, the variables time, t, and Q.

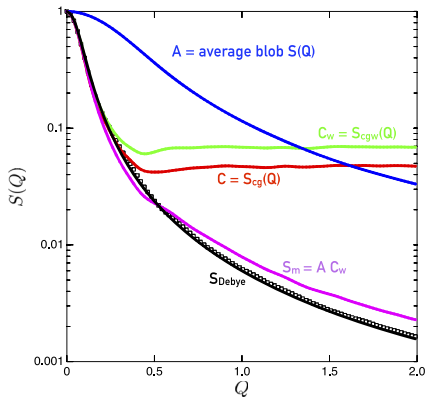

FIG. 1. Illustration (using simple Monte-Carlo simulation results) of the scattering contributions from a chain seen as a Gaussian random walk. Coarse graining to lumped centers at the "blob" level leads to a plateau (C) at higher Q in the initial Debye-function like chain scattering. Taking into account the variation of individual segment numbers in each blob between coarse graining steps along the chain leads to an additional fluctuation contribution that slightly elevates C to C_w. The difference between C_w and C is the fluctuation scattering amplitude that pertains to local reptation. In the plateau region, a constant ratio $C_w = (1+\Xi)C$ is encountered ($\Xi \simeq 0.41$). The blue curve (A) is the scattering due to the internal structure of the blobs, averaged over the blob-size distribution. The long chain Debye-type scattering [black symbols: MC results, black line: Debye $S(Q)$] can then be approximated by the multiplication $S_m(Q) = A(Q) \times C_w(Q)$ (magenta line) of the coarse grained chain scattering C_w and the blob scattering A. The Q-scale pertains to a segment length of 1. The example shown further assumes $N = 2000$, Gaussian random walks, and a coarsening step length of 35.

B. Rouse contribution—The dynamics of a Rouse blob limited by the tube

We treat the supposed Rouse motion within the tube in terms of a Rouse blob of a size assumed to be the lateral tube dimension. Setting aside translational diffusion, the dynamic structure factor for the Rouse blob reads

$$S_{\text{Rouse}}(Q,t) \cong \frac{1}{N_{\text{blob}}} \sum_{i,j}^{N_{\text{blob}}} \exp\left[-\left(\frac{Q^2}{6}\right)\left\langle [r_i(t)-r_j(0)]^2\right\rangle\right], \tag{11}$$

with

$$\left\langle [r_i(t)-r_j(0)]^2\right\rangle = |i-j| l_{\text{seg}}^2 + \frac{4R_e^2}{\pi^2} \sum_{p=1}^{N_{\text{blob}}} \frac{1}{p^2} \times \cos\left(\frac{p\pi\, j}{N_{\text{blob}}}\right)\cos\left(\frac{p\pi\, i}{N_{\text{blob}}}\right)[1-\exp(t\,\Gamma_p)], \tag{12}$$

where $\Gamma_p = 2W[1-\cos(p\pi/N_{blob})] \simeq p^2/\tau_R$ with $\tau_R \equiv \tau_e = R_e^4/(\pi^2 W l^4)$ and R_e being the size of the Rouse blob in terms of its end-to-end distance. We note that the "plateau level" of the dynamic structure factor is more sensitive to the tube cross section $\sim R_e^2$ than to the tube step length $l_{seg}\sqrt{N_e}$. The default interpretation infers $R_e = l_{seg}\sqrt{N_e}$; considering independent values of R_e and N_e may allow a heuristic and tentative assessment of possible asymmetries between both tube step length and width, i.e., stretching of the Rouse blobs along the contour. Later, in corresponding fits, this is realized by a factor f between these lengths

$$R_e = f\, l_{seg}\sqrt{N_e}, \tag{13}$$

where the plain default is $f = 1$. However, our considerations leading to the value of Ξ in Eq. (10) imply $f = 1$, a tentative variation of f would allow us to corroborate the value or possibly find hints to deviations between entanglement step length and R_e. The Rouse contribution depends on two parameters: the Rouse rate $Wl_{seg}^4 \equiv Wl^4$ and the blob size R_e.

The full dynamic structure factor, including local reptation and local Rouse dynamics, is calculated in terms of an incoherent approximation equivalent to a convolution of the correlation functions in real space and correspondingly to a product in (Q,t) space

$$S_{chain}(Q,t) = S_{Rouse}(Q,t)S_{tube}(Q,t), \tag{14}$$

and further, including the correlation loss due to contour-length-fluctuation (CLF) effects, we finally arrive at

$$S_{chain}(Q,t) = S_{Rouse}(Q,t)S_{tube}(Q,t)\;\; S^{CLF}(Q,t). \tag{15}$$

In the here used contrast labeling of a few protonated-chains (≃5%–10%) in a matrix of chemically equal deuterated-chains, NSE observes the normalized scattering function $S_{chain}(Q,t)/S_{chain}(Q,0)$.

To arrive at a consistent description of $S(Q,t)$, the rate parameters W of local reptation [Eqs. (8) and (9)] and Rouse (11) must correspond.

C. Assigning non-Gaussianity

Motivated by our recent results on the motion of short tracer chains in highly entangled melts,[40] which clearly showed non-Gaussianity effects, we also incorporated this into the expression for the Rouse type blob dynamics. This again has to be considered as a tool to inquire about the experimental results on the presence of non-Gaussianity effects by comparing the corresponding model computation with the experimental results.

In her paper on "Localization of Chain Dynamics in Entangled Polymer Melts," Guenza[21] came to the conclusion that the chain dynamics is non-Gaussian, which she described in terms of a non-Gaussian parameter $\alpha(t)$.[21] The scattering function becomes

$$S(Q,t) \cong \frac{1}{N_{blob}}\sum_{i,j}^{N_{blob}} \exp\left[-\left(\frac{Q^2}{6}\right) f\left(Q^2\right)\left\langle[r_i(t)-r_j(0)]^2\right\rangle\right], \tag{16}$$

with

$$f\left(Q^2\right) = 1 - Q^2\alpha(t)\left\langle[r_m(t)-r_m(0)]^2\right\rangle/12 + \mathcal{O}(q^4), \tag{17}$$

in order to avoid zero crossings for larger Q and t-values due to missing terms $\mathcal{O}(q^4)$ in Eq. (17), interpreting $1-(Qr)^2$ as a series expansion of $\exp\{-(Qr)^2\}$, we rather use

$$f\left(Q^2\right) \simeq \exp\left\{-Q^2\alpha(t)\left\langle[r_m(t)-r_m(0)]^2\right\rangle/12\right\}. \tag{18}$$

Thereby, $\left\langle[r_m(t)-r_m(0)]^2\right\rangle$ relates to the mean squared displacement. For a Rouse chain, we have

$$\left\langle[r(t)_m - r_m(0)]^2\right\rangle = \frac{1}{N_{blob}}\frac{4N_{blob}l_{seg}^2}{\pi^2}\sum_{n,p=1}^{N_{blob}}\frac{1}{p^2}\cos\left(\frac{p\pi\, n}{N_{blob}}\right)^2 \times\left[1-\exp\left\{-2W\left(1-\cos\left(\frac{p\pi}{N_{blob}}\right)\right)t\right\}\right]. \tag{19}$$

It remains to find an expression for $\alpha(t)$. Inspired by the simulation results of Guenza, we use a logarithmic Gaussian function

$$\alpha(t) = \alpha_0\, \exp\left[-\left\{(\ln[t]-\ln[t_{max}])^2/(2\sigma^2)\right\}\right], \tag{20}$$

with $\alpha_{max} = \alpha_0$; and $\sigma\ (= t_w)$ being the width of the distribution.

Following our diffusion experiment of short tracers in a highly entangled melt, we found that non-Gaussian behavior is limited to the chain dynamics within the tube; therefore, we used the entanglement blob time as t_{max}.

This augmentation of the plain Rouse sum equations (11) and (12) for the blob dynamics, together with the modified local reptation in the following, is used to fit the available NSE data.

D. Note on the role of Rouse rate determination

The Rouse rate determines the time scale of the polymer relaxation spectra, and independent prior knowledge would contribute to the corroboration of the proposed new model and reduce the uncertainties of other parameters as, e.g., the tube dimensions. The slope in the plateau regime (of local reptation), which relies on how W enters the local reptation time scale, **and** the short time regime, which significantly depends on the blob Rouse rate, have to be consistent. Unfortunately, this parameter is not well known for most of the considered polymers, in particular for the temperatures of the NSE experiments and the high molecular weights. Using plain (long

TABLE I. Basic conformational and rheological parameters for the five investigated polymers: M_e: entanglement molecular weight; N_e: number of monomers in an entanglement strand; M_0: monomer molecular weight; C_∞: characteristic ratio; d_{rheo}: tube diameter from rheology; l_{seg}: monomer length $l_{seg}^2 = n_b C_\infty l_0^2$ with n_b: number of bonds/monomer; l_0: bond length; and T(rheo): reference temperature of the rheological measurement.

Polymer	M_e (g/mol)	N_e	M_0 (g/mol)	C_∞	d_{rheo} (Å)	l_{seg} (Å)	T(rheo) (K)
PEO190	1624	36.9	44	4.8	34.5	5.68	413
PEP200	2284	33.7	70	6.4	43.3	7.46	413
PE190	828	59	14	7.3	31.1	4.05	413
1-4 PB45	1815	34.8	54	5.3	40.0	6.78	413
PI350	5429	82.9	68	5	60	6.59	298

TABLE II. Results of fitting the NSE-spectra for times $t > \tau_e$ from five polymer melts with Eq. (2). Wl^4: Rouse rate; d_{DG}: tube diameter from Eq. (2); $W = (Wl^4)/(l_{seg}^4)$; T is the temperature of the NSE experiments; and χ^2: normalized sum of errors. * estimated from temperature-shifted short chain rheology data.

Polymer	Wl^4 (Å^4 ns^{-1})	d_{DG} (Å)	W (ns^{-1})	T (K)	$t_s \simeq \tau_e$ (ns)	χ^2
PEO190	14 890	47.6 ± 0.16	14.3	413	33	1.8
PEP200	32 600	60.2 ± 0.2	10.4	473	44	2.6
PE190	70 000	48.8 ± 0.1	260	509	8	2.9
1-4 PB45	22 700	52.2 ± 0.33	10.7	423	34	2.7
1-4 PB45 (CLF)	22 700	49.0 ± 0.33	10.7	423	34	2
PI350	4000–6000*	77. . .71	2.1. . .3.2	400	180	30. . .28

chain) Rouse dynamics as a model to extract Wl^4 from the short time range of $S(Q,t)$ of long chain polymers—as hitherto common - often results in—possibly ignored or overlooked—wrong slopes in the long time local reptation regime. Typically, this is more obvious if data are displayed on a log time scale than in the conventional linear plots of $S(Q,t)$ vs t (see, e.g., the discussion on Rouse rate determination for PI in the supplementary material).

This—besides the observation of a deviating stretched exponential approximation at short times with a stretching exponent of $\beta \simeq 0.5$ rather than 0.83[39]—indicates that some combination of Rouse blob and local dynamics has to be used for a proper description of the short time dynamics.

Application of expressions from the plain Rouse model to extract Wl^4 from viscosity, diffusion, or even NSE spectra may need

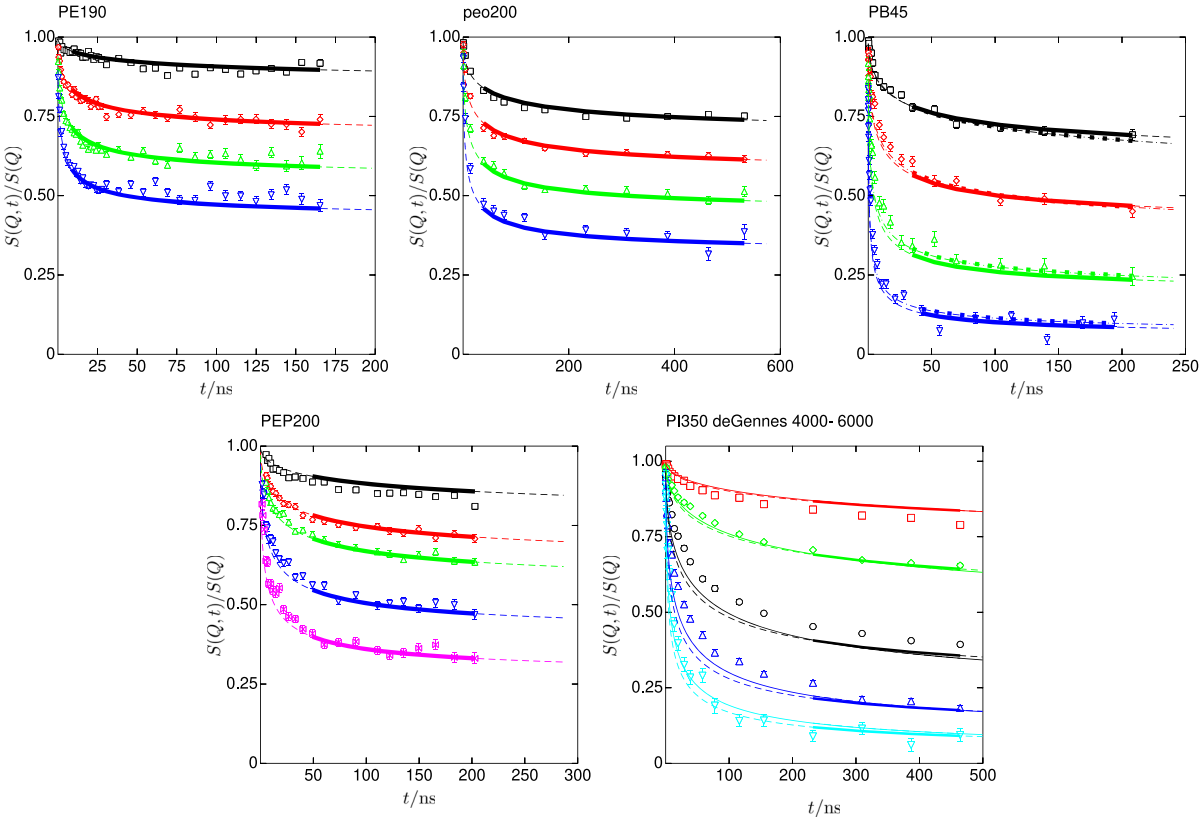

FIG. 2. Fits for PE190, PEO200, PB45, PEP, and PI with Eq. (2) to the spectra from the five different polymers. The results are shown in Table II; thick solid lines: fitted parts; thin dashed lines: Eq. (2) computed over the full time range. For PB45, fits using Eq. (2) (solid and dashed lines) and Eq. (4) (dotted and dashed-dotted lines) are displayed. Q-values always from above: (a) 0.05, 0.77, 0.96, and 0.115 Å^{-1}; (b) 0.078, 0.96, 0.115, and 0.137 Å^{-1}; (c) 0.08, 0.11, 0.15, and 0.2 Å^{-1}; (d) 0.05, 0.068, 0.077, 0.096, and 0.115 Å^{-1}; and (e) 0.053, 0.073, 0.104, 0.135, and 0.167 Å^{-1}. Note: the lines and dashed lines for PB45 indicate results with and without CLF, and for PI350 (4000 and 6000), they represent results for Wl^4 = 4000 or 6000 Å^4/ns.

extrapolation using the temperature shift factor and, in any case, correction factors to account for a M_w dependence. This is best investigated in the case of polyethylene, but even there, the results obtained by different approaches differ considerably and just yield the right order of magnitude.

Values for the Rouse rate may be inferred from NSE-measurements on low molecular melts (M_w below the entanglement regime); those values, however, would need to be extrapolated to larger M_w since for small molecular weights the Rouse rate depends on chain length[22] (see discussion in the supplementary material). Another approach may rely on the viscosity from rheology experiments in the Rouse regime, possibly with the Williams–Landel–Ferry temperature shifted to the NSE temperature. If the former methods are not available, the interpretation of NSE–data on the entangled polymer melts typically assumes that the initial (short time decay) of the available long chain melt $S(Q,t)$ could be used to extract Wl^4 by fitting a simple Rouse structure factor to the initial decay, typically limited to times $< \tau_e$. However, it seems that in favorable cases (e.g., PE), the associated error of this procedure is low and the Wl^4 values stay consistent, this is not a universal feature.

In the supplementary material, the previous (literature) knowledge on Rouse rates for various polymers is presented and contextualized in the present study. Where accurate Rouse rates from independent measurements were not available, we used previous estimates (Table II) as starting points for consistent fits with the full model as presented in this work.

IV. EXPERIMENTS AND DATA EVALUATION I

First, we use the well-known DeGennes approximation Eqs. (1) and (2) to reevaluate five different polymers that were investigated by NSE over the recent years, namely polyethylene (PE),[29,41] polyethylene-alt-propylene (PEP),[42] poly(ethylene oxide) (PEO),[44] polybutadiene (PB),[45] and polyisoprene (PI); see the supplementary material (page 1). For these polymers, we dispose of precise structural as well as rheological data. Table I subsumes these results.[46]

The melt data from PE, PEO, PB, and PEP have been evaluated before in terms of Eq. (2).[25–29,31,32,40–42,44,47] PI was synthesized by anionic polymerization; the details including the characterization are described in the supplementary material.

The actual fit results from Eq. (2) are presented in Table II and shown in Figs. 2 and 3.

In each case, the fits were performed simultaneously for all available Q-values but such that the initial Rouse regime was omitted ($t > \tau_e$). The initial Rouse rates Wl^4 in Table II part had coarsely been estimated from fitting the short time dynamics with the Rouse model at $t < \tau_e$. Since this is not really consistent with the here presented model, a better way would be to use independent

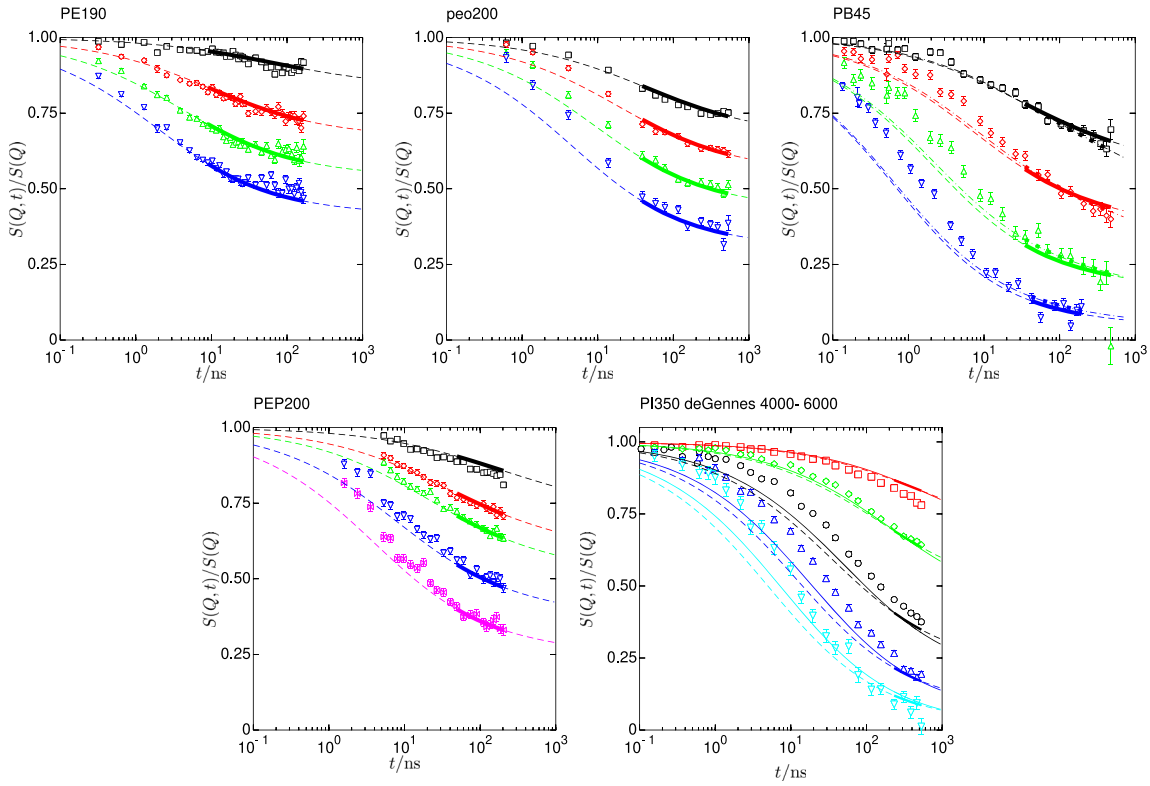

FIG. 3. Same as Fig. 2 but in semi logarithmic representation, highlighting the deviations at small times and slope errors in the plateau regime.

measurements to fix it, as discussed in Sec. III D; thus, the obtained values are given in the supplementary material. It turns out that the available extrapolated Wl^4 varies up to a factor of 2 and so just can corroborate the order of magnitude. Thus, finally, the best fits of the new model also need to fit the Wl^4 within the new model. Assuringly, in most cases, the obtained values are reasonable close to the anticipated ones; however, they are consistently somewhat lower (up to about 30%–40%).

In general, rather good fits in the long-time local reptation regime are already obtained with the "conventional" approach of Eq. (2) (see Figs. 2 and 3).

We note that the linear presentation graphs, though emphasizing the longer time local reptation regime, do not clearly show to what extent the fitting results represent the actual slopes of the data toward long times. Therefore, Fig. 3 shows the data from Fig. 2 in a semi logarithmic presentation. Figure 3 shows that for the first four polymers: PE, PEO, PB, PEP and also PI—if Wl^4 is estimated from rheological data (see Sec. II) rather than using the conventional Rouse fit to the initial slope region—Eq. (2) also nicely reproduces the slopes of the experimental data at longer times above τ_e in the local reptation regime. This, however, would not be the case for PI if Wl^4 as estimated by simple short time fits of the entangled polymer spectra were used (as illustrated in the supplementary material). With improved Wl^4 values, the slopes shown in Fig. 3 emerge. It is advisable in fitting polymer melts to check the slopes, in order to judge the validity of the data analysis, in particular the consistent determination of the rate parameter W.

As referred to in the theoretical part, a description of the PB chain dynamics (molecular weight of 45 kg/mol) needs to consider CLF. The dashed-dotted lines for PB in Fig. 2 show the outcome of a fit with Eq. (4); the achieved parameters are listed in Table II. From Fig. 2, one notices that the longer time slopes of the spectra are better described by Eq. (4) including CLF; the smaller χ^2 reflects this observation. Looking at the tube diameter, including CLF leads to a somewhat smaller d_{DG} compared to the fit with Eq. (1) (7% difference).

We note that here and in the following, χ^2 yields a reasonable comparison between different model variants applied to one polymer dataset. However, the relation of these values between different experimental datasets also depends on the statistical errors (measuring time) and the residual systematic errors (fluctuations) of the respective experimental datasets that are not included into the data errors. Lower statistical errors ("better data") typically lead to larger χ^2-values due to minor deficiencies in the model description or small additional systematic errors! Thus, the inter-polymer comparability of the absolute value of χ^2 is somewhat limited, in particular, since there are large time gaps between the experiments.

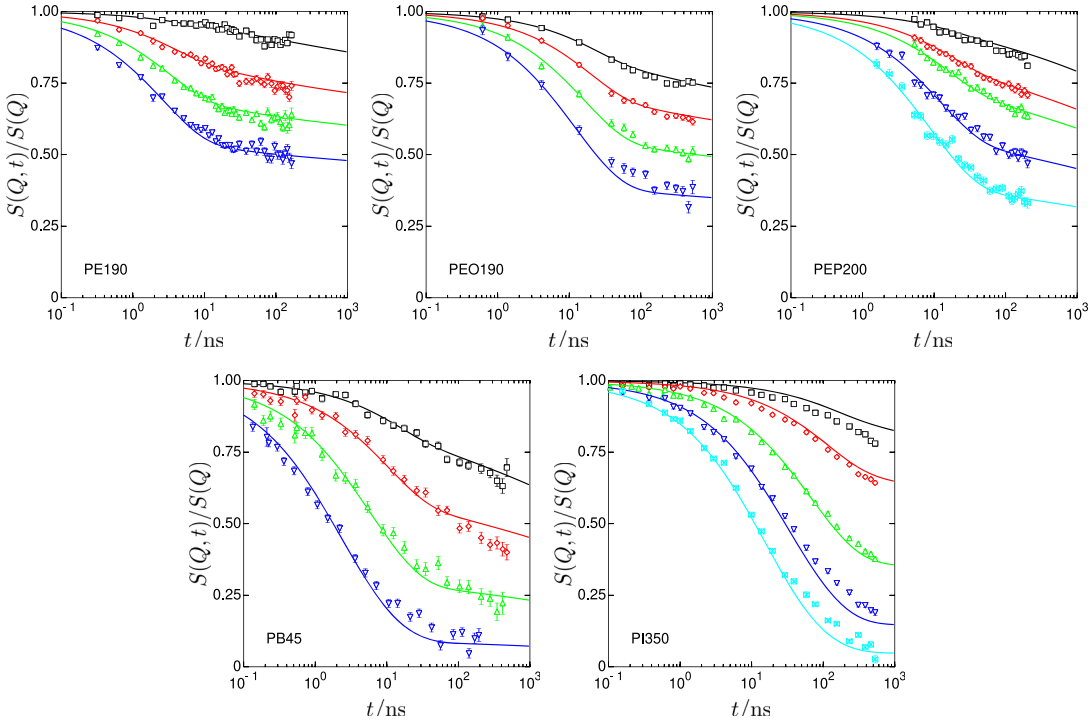

FIG. 4. Results of fits of the plain reptation model to NSE data with Q-values as in Fig. 2 using the model expression Eq. (10), in combination with (i.e., multiplied by) a plain blob-Rouse scattering (without non-Gaussianity effects) from a blob with $R_e = l\sqrt{N_e}$ and including a contour length fluctuation correlation loss contribution $S^{CLF}(Q,t)$, which, however, in the covered experimental range is only important for PB45. Except for PI350, the fits are already quite satisfactory. The resulting fit parameters are given in Table III, with Q-values as in Fig. 2.

V. DATA EVALUATION II: FULLY INTEGRATED DE GENNES STRUCTURE FACTOR COMBINED WITH ROUSE BLOBS

We now focus on fits using the convolution of the fully integrated De Gennes function after applying the coarse graining [Eq. (10)] with the dynamic structure factor for the Rouse blob [Eq. (11)] as expressed by Eq. (15). In order to get systematic and physically meaningful results, it is important to use all available prior knowledge. This concerns the structural parameters: l_{seg}; N, and a guide for start values for the dynamical parameters Wl^4. Wl^4 and N_e are listed in Tables I and II.

Furthermore, on short tracers in high molecular weight PE and PEO melts, we made observations that may be important for this study: (i) the dynamics of the tracers appeared to occur in a highly cooperative way with the long chain host. (ii) This cooperativity is limited by the tube size. (iii) In the "Rouse regime" at short distances or for a time shorter than τ_e, the spectral contribution of the internal tracer modes was much weaker than expected from the Rouse model. (iv) The reduction of the mode amplitudes may be understood in terms of non-Gaussian segment displacement distributions.[47]

These observations suggest that, for the entanglement blob of the long reptating chain, the Rouse picture of the initial chain relaxations within the tube may also need a corresponding modification.

A. Results of model fitting

The new model fitting to Eq. (15) was performed in several variants without and with non-Gaussianity (NG) correction [Eq. (19)], without ($f = 1$) and with (artificial) decoupling (f is a fit parameter) of the entanglement strand length N_e, and the lateral blob size R_e, approximating the effect of anisotropic longitudinal and lateral tube dimensions. The NG correction was applied with $t_{max} = \tau_e$ and $t_w = 1$ fixed, respectively (except for three alternative fit variants, PI350 also trying $t_{max} = 0.3\tau_e$). We emphasize that in all cases, the fitting simultaneously embraced the full available Q- and time ranges. The fit results are shown in Figs. 4 and 5, and the corresponding parameters are mentioned in Table III; the different variants are indicated by suffixes:

- (none): plain model [Eq. (15)] without NG correction ($\alpha_0 = 0$). The only basic fit parameters were N_e and Wl^4, as in all other variants (two parameter fits).
- -alpha0: plain model with active NG correction with $t_{max} = \tau_e$ and $t_w = 1$ fixed, the additional fit parameter is α_0 (three parameter fits).
- -alpha0-f: plain model with NG correction and allowing for a factor f between $l_{seg}\sqrt{N_e}$ and the blob size R_e; the additional fit parameter is f (four parameter fits).

In addition, for the more difficult case of polyisoprene (PI), we also employed the following further fit variants:

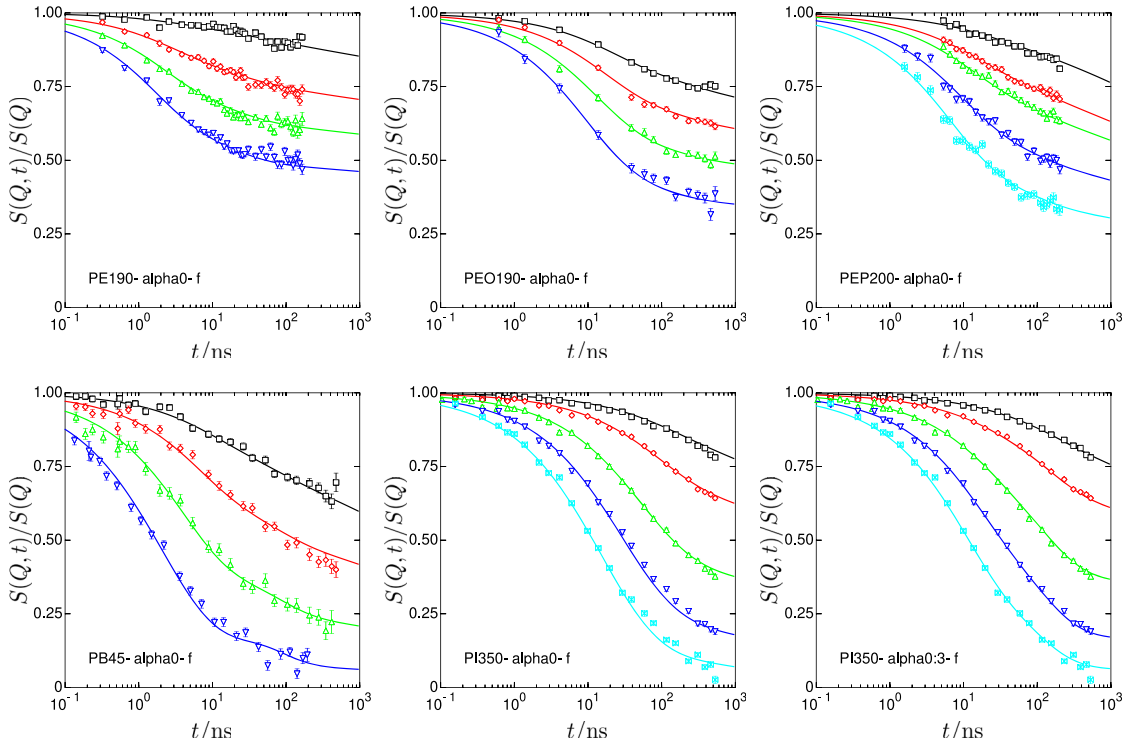

FIG. 5. Results of fits to NSE data in Fig. 4, but here including non-Gaussianity effects and a heuristic anisotropy factor f. The fit parameters are given in Table III. For PI, a fit with $t_{max} = 0.3\tau_e$ is shown. A complete display of all fit variants in the present vs $\log(t)$ as well as vs the t scale is shown in the supplementary material.

TABLE III. Fit results obtained with the dynamic structure factor for local reptation (fitted parameters are indicated by error specification following ±) combined with Rouse motion within the tube according to Eq. (15). Suffixes -alpha0 indicate non-Gaussianity inclusion: (α_0 fit, with: 3 → $t_{max} = 0.3\tau_e$ fixed and -w: t_w fitted); and the suffix -f indicates that f is fitted (f = factor between d_{tube} and blob size R_e). Note that in all other cases, $d_{tube} = R_e$.

Polymer	d_{tube} (Å)	R_e (Å)	Wl^4 (Å^4/ns)	α_0	t_{max} (ns)	t_w (ns)	$\langle\chi^2\rangle$
PE190	48.7 ± 0.1	48.7	60 577 ± 1201	···	···	···	2.85
PE190-alpha0	49.8 ± 0.2	49.8	66 087 ± 1643	0.06 ± 0.01	9.4	1.0	2.30
PE190-alpha0-f	49.5 ± 0.9	49.8 ± 1.4	66 462 ± 1983	0.06 ± 0.01	9.4	1.0	2.30
Average ± var	49.3 ± 0.4	49.4 ± 0.5	64 375.16 ± 2 690.42	0.06	9.4 ± 0.0	1.0	···
PEO190	48.5 ± 0.2	48.5	9765 ± 348	···	···	···	2.27
PEO190-alpha0	49.5 ± 0.3	49.5	10 458 ± 446	0.06 ± 0.01	58.0	1.0	1.58
PEO190-alpha0-f	59.3 ± 2.5	47.8 ± 3.0	9226 ± 472	0.04 ± 0.01	57.4	1.0	1.20
Average ± var	52.4 ± 4.9	48.6 ± 0.7	9 816.21 ± 504.33	0.05 ± 0.02	57.6 ± 0.3	1.0	···
PEP200	57.2 ± 0.2	57.2	25 487 ± 545	···	···	···	2.05
PEP200-alpha0	59.8 ± 0.6	59.8	25 633 ± 795	0.08 ± 0.01	50.4	1.0	1.42
PEP200-alpha0-f	65.1 ± 1.4	57.4 ± 2.2	24 328 ± 734	0.05 ± 0.01	45.3	1.0	1.26
Average ± var	60.7 ± 3.3	58.1 ± 1.2	25 149.26 ± 583.76	0.06 ± 0.02	46.1 ± 3.3	1.0	···
PB45	48.4 ± 0.3	48.4	15 859 ± 348	···	···	···	2.78
PB45-alpha0	50.8 ± 0.5	50.8	16 029 ± 399	0.09 ± 0.01	42.1	1.0	1.73
PB45-alpha0-f	55.2 ± 1.9	49.5 ± 2.9	15 776 ± 412	0.08 ± 0.01	38.5	1.0	1.68
Average ± var	51.5 ± 2.8	49.6 ± 1.0	15 887.84 ± 105.57	0.09 ± 0.01	38.5 ± 2.9	1.0	···
PI350	64.5 ± 0.2	64.5	5364 ± 54	···	···	···	18.69
PI350-alpha0	73.0 ± 0.6	73.0	4951 ± 61	0.11 ± 0.01	579.7	1.0	13.65
PI350-alpha0-f	122.7 ± 2.8	62.0 ± 2.4	4921 ± 64	0.03 ± 0.01	303.9	1.0	3.59
PI350-alpha0:3	79.9 ± 0.5	79.9 ± 0.5	4948 ± 53	0.14 ± 0.00	275.6	1.0	8.99
PI350-alpha0:3-f	150.2 ± 3.5	61.3 ± 2.1	4898 ± 73	0.05 ± 0.00	96.2	1.0	1.72
PI350-alpha0:3-w	77.2 ± 0.6	77.2	6339 ± 119	0.14 ± 0.00	187.5	3.5 ± 0.4	6.99
Average ± var	94.6 ± 31.0	69.6 ± 7.4	5 237.00 ± 518.12	0.1 ± 0.05	295.1 ± 149.3	1.4 ± 0.9	···

- -alpha0:3: plain model with NG correction, but with the modification $t_{max} = 0.3\tau_e$.
- -alpha0:3-f: plain model with NG correction as mentioned above and allowing for a factor f between $l_{seg}\sqrt{N_e}$ and R_e.
- -alpha0:3-w: plain model with NG correction as mentioned above and allowing a fit of t_w.

The three latter variants are prompted by the deviations observed for PI350, namely the tendency of the fits to create a NG-$\alpha(t)$ related unphysical peak at times somewhat beyond the observation range. A reliable estimate of the strength of $\alpha(t)$ is undependable in this situation. Note that—except for PI350—the two-parameter plain model already yields quite good fits of $S(Q,t)$ over the whole covered (Q,t)-range; with the additional non-Gaussianity amplitude as the third parameter, the minor residual deviations are also removed. Additions of further variants were tested in order to explore the potential nature of the deviation observed in the PI350 data.

All resulting parameters are listed in Tables III and VI; all values with specified statistical errors were fitted, and the others were fixed. Note that these errors pertain to statistical counting errors only.

Let us now inspect the results obtained from the fit variants for the different polymers in some detail.

PE: If we compare the fitting results shown in Figs. 4 and 5, we find only minor differences in the visual fit quality. However, in Fig. 4, minor deviations in the sequence of spectra between data and fitting curves are visible, the full fit shown in Fig. 5 shows perfect agreement. We note that varying t_{max} does not affect the results. Probing deviations that could be related to tube asymmetries (by also fitting f) lead to $f = 1.006 \pm 0.02$ (i.e., no indication of any asymmetry).

The fitted Rouse rate Wl^4 values of $6 \ldots 6.6 \times 10^4$ Å^4/ns stay slightly below the previous estimate of 7×10^4 Å^4/ns from Table II.

The tube diameter d_{DG} obtained from the simple fit with Eq. (2) agrees well with $d_{tube} = R_e$ in our model formulation.

PEO: The fits for PEO show a very similar outcome as those for PE. Similar to PE, the simple fit varying only Wl^4 and N_e already describes the PEO spectra rather well, and again the full fit leads to perfect agreement. In particular, visible residual deviations at intermediate times and large Q are removed by the inclusion of NG-corrections, indicating the presence of non-Gaussianity.

As for PE, the lateral tube dimension R_e is robust, while the tube step-length varies if we probe the anisotropy variable $f = 0.81 \pm 0.04$, however, with less effect on d_{eff} (see Table III), while R_e of the plain model fit virtually matches the PE-value and is only marginally larger (2%) than the previously determined d_{DG}-value.

The Rouse rate yielded by the fits $Wl^4 = 0.92 \ldots 1.05 \times 10^4$ Å^4/ns is again somewhat lower than the initial estimate of 1.49×10^4 from Table II.

PEP: As Fig. 4 shows, the simple plain model already reproduces the data quite well; close inspection, however, indicates that the Q-dependence is still slightly off and also the shape at intermediate Q displays minor but visible deviations. The full fit including non-Gaussianity correction, on the other hand, again perfectly describes the data. The possible anisotropy measure $f = 0.88 \pm 0.03$ still stays close to 1.

The Rouse rate $Wl^4 = 2.5 \times 10^4$ Å^4/ns is stable against the different fitting variants and again lower than the previous estimate of 3.26×10^4 (Table II). Inclusion of NG-correction significantly improves the fit.

PB: Again, the plain-model fit shown in Fig. 4 shows a fair agreement, but also shows some deviations at larger (Q, t). On the other hand, the full fit is able to reproduce the data to a large extent, basically because of the non-Gaussianity corrections. Probing f yields $f = 0.9 \pm 0.04$, i.e., close to 1.

The Rouse rate and the lateral tube dimension are rather stable against fit variants.

In addition, $Wl^4 \simeq 1.59 \times 10^4$ Å^4/ns is again somewhat lower than the initial estimate (Table II) of 2.3×10^4.

PI: PI poses the most problems for our model-fit approach. However, the plain model fit still approximately reproduces the salient features of the curves, the Q-dependence of the data seems to be weaker than that of the model, and the shapes with a larger t also show deviations. By including non-Gaussianity and tweaking the anisotropy factor $f \simeq 0.5$, perfect fitting may be achieved as shown in Fig. 5. The resulting tube size parameter shows considerable variation between different approaches, in particular, with and without the heuristic anisotropy factor f. Nevertheless, they embrace the previous d_{DG} estimate.

The Rouse rate Wl^4 is about 5000 and is in the range of the previous estimates (Table II).

The more difficult fitting of PI probably pertains to the limitation of the experimental time range to only a few τ_e, thereby not providing a genuine probing of the local reptation regime.

In summary, we observe that the plain model already yields a fair representation of the available NSE data of long reptating polymer chains. However, closer inspection strongly indicates that non-Gaussianity effects on the "blob"-level play an important role. Somewhat weaker (and in terms of a heuristic approach) are indications for a slightly anisotropic tube in some polymers. In particular, the fits of the PI data show a trend toward $f < 1$.

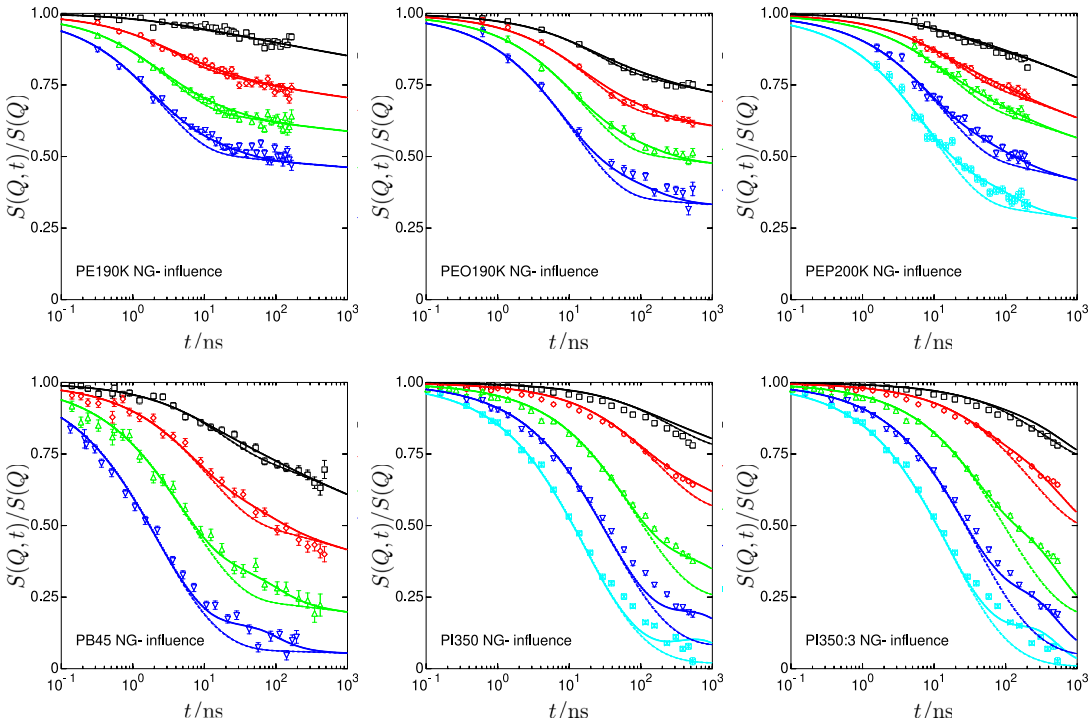

FIG. 6. Illustration of the influence of the NG-correction on $S(Q,t)$ using the parameters of the -alpha0 variants yielding fit results as shown by the solid lines compared to $S(Q,t)_{\alpha_0=0}$ with the same parameters except for the setting $\alpha_0 = 0$ (dashed lines).

In all cases, the values of Wl^4 are quite robust and smaller than the previous estimates.

Within small total variations (uncertainties of 1 to 2 Å) the analysis yields consistent values of the tube diameter d_{eff}. Thus, the microscopic observation by NSE reliably delivers the microscopic confinement volume $V_{conf} = d_{\mathrm{eff}}^3$ $\left(d_{\mathrm{eff}} = \sqrt{(d_{\mathrm{NSE}}^2 + 2R_{\mathrm{e}}^2)/3} = l_{\mathrm{seg}}\sqrt{N_{\mathrm{e}}(1+2f^2)/3}\right)$, which is established by the topological constraints. Even if we allow for the heuristic anisotropy factor f, d_{eff}, generally, is significantly larger than d_{rheo}, an observation that was already made by the more simple evaluations in terms of Eq. (2). In addition, the tube step-lengths determined by NSE, d_{NSE}, in most cases, are nearly twice the rheological values.

B. Modified local reptation and non-Gaussianity

As seen above, the fits with the plain local reptation model ansatz [Eq. (15)] may be further improved by activation of non-Gaussianity corrections. The inclusion of NG-corrections is very much in line with earlier results on tracer diffusion and simulations and theoretical results on the basis of a generalized Langevin equation (GLE) by Guenza.[21] NG-corrections significantly reduce the χ^2 values for all polymers (see Table III). We note that the amount of NG-correction differs by a factor of about 2 if expressed by the values of the amplitude α_0 [Eq. (20)] between the different polymers. The smallest corrections ($\alpha_0 \simeq 0.06$) are found for PE and PEO; for the other cases, nearly all NG-including fits yield $\alpha_0 \simeq 0.08\ldots0.13$. The correction to the Rouse relaxation is a retardation close to $t = t_{\max}$ and the maximum suppression depends on α_0. The strength and visibility of the correction increase with Q^2, and its influence is centered around $t = t_{\max} \simeq \tau_{\mathrm{e}}$. The time dependence and magnitude of the non-Gaussian correction to the blob-Rouse dynamics accordingly may be assessed by comparing the curves with and without NG-correction shown in Fig. 6.

Note that the correction has a tendency to yield a bump in $S(Q,t)$ relaxation curves at large Q and $t \simeq t_{\max}$, which for large α_0 may even develop into an unphysical peak. Therefore, a caveat must be taken in this realm, which pertains to the fact that the NG correction expression is based on a series expansion in Q^2, truncated beyond the first Q^2 term. At larger (Q,t), the relevant variable $Q^2\langle r_{mm}^2(t)\rangle$ may lead to a regime, where the series expansion breaks down. Since, we lack any information on higher order expansion terms, the details at larger (Q,t) should be interpreted with appropriate caution. Extending experiments further in this regime may give more insights but is beyond our current scope.

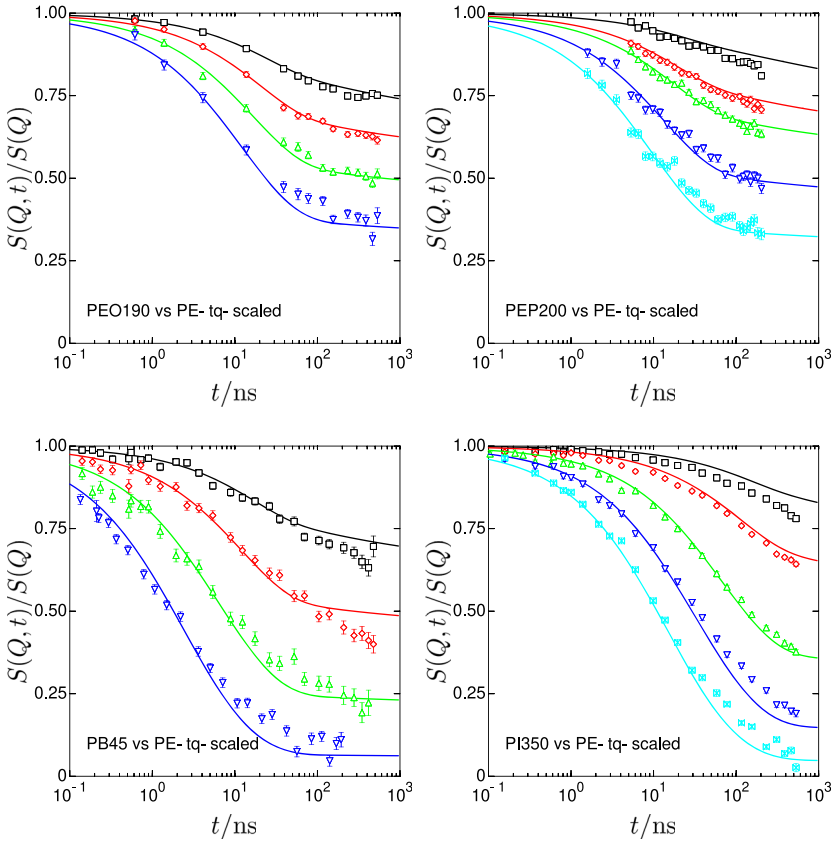

FIG. 7. Comparison of the scaled (q and t) computed spectra to the PE190 using the scale factors as fit parameters. The resulting factors are given in Table IV.

C. Generic properties

In the following, we compare spectra from different polymers in order to shed light on the extent of the universal generic behavior of their spectra in the local reptation regime. Due to individual differences in length- and time-scales, the comparison requires appropriate scaling of the respective Q (1/length) and times for the juxtapositions of $S(Q,t)$'s. The excellent interpolation provided by model fitting to Eq. (15) (irrespective of parameter interpretation) for all of our reptation type scattering functions allows an independent approach to assess the scaling properties that overcomes the difficulties posed by the fact that the (Q,t) points where the NSE data of the different polymers were measured in the time-span of three decades do not exactly match.

For this purpose, $S(Q,t)_{\mathrm{p1}}$ of polymer p1 is computed (interpolated, using previously determined model parameters) at the $(Q_{\mathrm{p2,i}} \times q_{\mathrm{scale}}, t_{\mathrm{p2,j}} \times t_{\mathrm{scale}})$-points with the experimental $q_{\mathrm{p2,i}}$ and $t_{\mathrm{p2,j}}$ values of the polymer p2 data and fitted scaling factors q_{scale} and t_{scale}. The comparison of the (Q,t)-scaled model representation of one polymer to the data of another polymer is shown in Fig. 7. Since the model representation is more accurate if used for interpolation within the experimentally covered (Q,t) regime than extrapolation beyond, the preferred combination of p1 for polymer data and p2 for model representation may be chosen accordingly. However, both directions yield consistent results.

Thus, the obtained scaling results using the model parameters of PE as reference are shown in Fig. 7 and the corresponding scaling factors are listed in Table IV.

In Table V, we compare the tube diameters that would result from multiplying the PE-reference tube size with q_{scale} and the Rouse rates resulting from multiplying the PE-reference Rouse rate by t_{scale}. However, the inferred tube diameters are close to the previously fitted values, the simply scaled Rouse rates grossly differ from the expected values if the tube diameters are not the same. It is obvious that scaling Wl^4 with $t_{\mathrm{scale}} \times q_{\mathrm{scale}}^4$, i.e., scaling time according to the τ_e-ratios, again yields close matches.

Thus, the t-scaling reveals that the relevant quantity for scaling is not simply Wl^4 but rather the Rouse rate of the entanglement blob $\tau_e = d^4/(\pi^2 Wl^4)$, i.e., $t_{\mathrm{scale}} = \tau_{\mathrm{e}/\tau_{\mathrm{e,ref}}}$. That is, the implied scaling may be subsumed as follows:

$$S(Q,t) = S_{\mathrm{ref}}(Q \times \{d/d_{\mathrm{ref}}\}, t \times \{\tau_{\mathrm{e}}/\tau_{\mathrm{e,ref}}\}), \tag{21}$$

where the index *ref* pertains to any chosen reference polymer (or scattering function model), and $S(Q,t)$, d, and τ_{e} are the parameters of the scaling "target."

TABLE IV. Scale factors for time and wave-vector (length scale) as obtained by fitting the factors applied to an interpolation (using plain model parameters) of one polymer (PE) to the data of another polymer.

Polymer	t_{scale}	q_{scale}	χ^2
PEO190	0.161 ± 0.007	1.002 ± 0.003	2.5
PEP200	0.193 ± 0.006	1.230 ± 0.004	3.5
PB45	0.219 ± 0.008	1.055 ± 0.006	4.2
PI350	0.029 ± 0.0006	1.327 ± 0.004	19.7

TABLE V. Comparison of tube diameters and Rouse rates resulting from scaling with the factors given in Table IV with fit results from Table III. All parameters pertain to the plain model fits.

	$d_{\mathrm{eff}}^{\mathrm{scaled}}$ (Å)	$d_{\mathrm{eff}}^{\mathrm{fit}}$ (Å)	$Wl^{4\ \mathrm{scaled}}$ (Å^4/ns)	$Wl^{4\ \mathrm{scaled}}$ $[\mathrm{d_x/d_{ref}}]^4$	$Wl^{4\ \mathrm{fit}}$ (Å^4/ns)
PE ref	(48.7)	48.7	(60 577)		(60 577)
PEO	48.6	48.5	9 753	9 831	9 765
PEP	59.9	57.2	11 691	26 759	25 487
PB45	51.1	48.4	13 266	16 434	15 859
PI350	66.8	64.5	1 756	5 477	5 364

The latter was an unexpected observation, which, however, is also corroborated by computational checks of the plain-model function. The numerical scrutinization of Eq. (14) reveals that for large N and in the relevant span of tube diameters covering at least $d = 20 \ldots 100$ Å, $d = R_e = l_{\mathrm{seg}}\sqrt{N_{\mathrm{e}}}$ and τ_e-scaling is virtually perfect (see the supplementary material) and obviously corroborated by the measured data.

In order to further verify this behavior, the combined (Q,t) scaling was fixed to the above-mentioned relation, and comparisons were made by solely fitting the d-value, implying the time scale from the previously determined Rouse rates and the resulting τ_e ratios. We note that despite some residual ambiguity in the choice of the "previously" determined Rouse rates, the model variants all yield Wl^4-values that are consistent within a few percent. In the following, we assume the Rouse rate values obtained by the plain-model fits.

Results to illustrate the degree of scaling goodness are given in Fig. 8. This may also be devised as a tool to provide an accurate relation of tube diameters between different polymers, irrespective of the exact definition of the absolute diameter values. Taking PE as reference with $d = 48.5$ Å, we thereby get, by a most basic plain comparison (no differences in NG-corrections included): $d/\text{Å} = 48.9$ (PEO), 60.2 (PEP), 51.7 (PB), and 64.9 (PI).

Residual differences (most visible for PI350 compared to the other polymers) are largely to be assigned to polymer specific differences in (local) non-Gaussiantiy and/or—where the q-sequence tends to be slightly weaker or stronger—may indicate a tube asymmetry.

Summarizing, we note that all polymer spectra display virtually the same generic properties, such as they are scalable with respect to each other if the time variable is related to the ratio of the Rouse times τ_{e} of the entanglement blobs, while the relevant length scale is the ratio of the tube diameters d_{NSE}.

D. The tube size parameters

In the following, we discuss the relation between the parameters characterizing the tube confinement both along the tube step length d_{NSE} and the lateral size characterized by R_{e}. Table VI lists the corresponding parameters that resulted from the different types of modeling for the different polymers and relates them to each other.

From the model formulation, we have a direct correspondence with the tube step length $d_{NSE} = l_{\mathrm{seg}}\sqrt{N_{\mathrm{e}}}$ and the "blob"-size R_{e}, which rather pertains to the lateral tube extension. Here, we refer

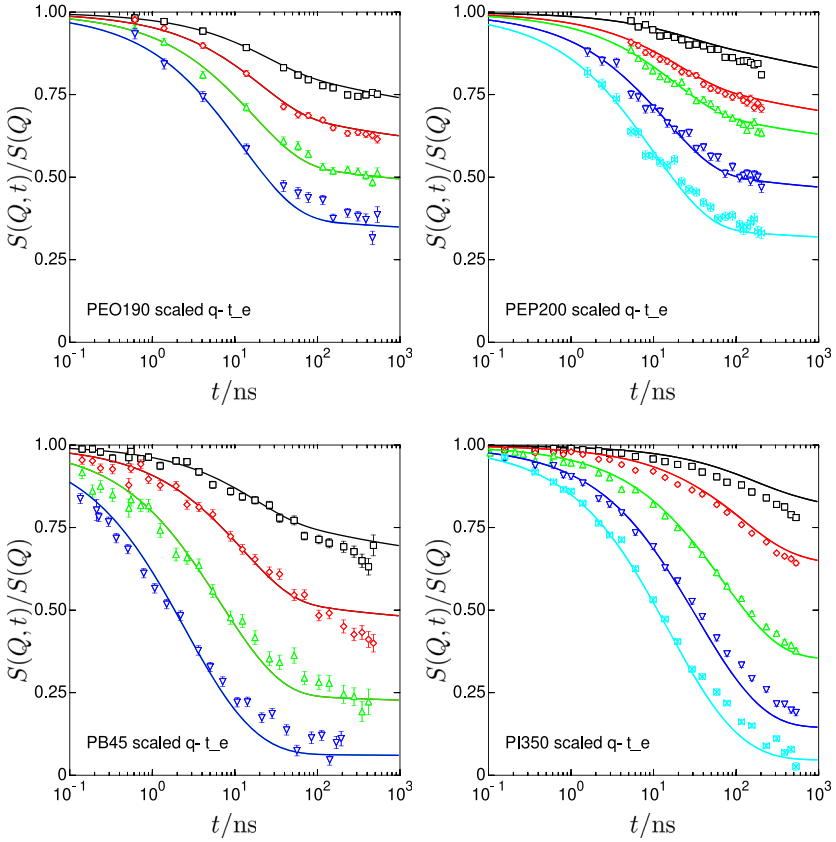

FIG. 8. Comparison of the *d*-scaled PE-model (qd and t/τ_e) spectra to the NSE data of different polymers. The matching is virtually indiscernible from that shown in Fig. 7. Note that the main deviations are seen in the influence zone of the NG-corrections, which seem to differ between the different polymers. In addition, here, it is visible that the PI350 exhibits the worst matching.

to the angular averaged "blob" $S(Q)$ for the interpretation of R_e as lateral tube diameter. However, in detail, the tube model with steps along the contour implies some stretching of the "blobs." Heuristically, in our model, this is expressed by having the factor $f = d_{NSE}/R_e \neq 1$ to account for a possible anisotropy of tube length parameters.

From Table VI, we observe that for all polymers, the microscopic step length of the tubes d_{NSE} and the lateral dimensions R_e are systematically larger than their rheological counterparts d_{rheo}. On average, d_{rheo} amounts to about 60% to 70%(80%) of d_{NSE} (R_e).

The second general observation regards the relation between the lateral tube size R_e and the step length d_{NSE}. For all polymers, the factor f between d_{NSE} and R_e is smaller than 1 (however, only insignificantly for PE, PEO, PEP, and PB but down to 0.5 for PI). In a heuristic way, we may tentatively interpret this behavior such that the lateral tube size R_e is narrower than its step length: the tube is asymmetric, i.e., leaner in the lateral direction. Kröger and his group have analyzed MD-simulations on PE and PB chains[49] with the aim to differentiate between the tube step length and the lateral tube dimension. For all simulations, they also find a larger step length compared to the lateral size. For PE (400 units), the ratio corresponding to R_e/d_{NSE} amounted to 0.74; for *trans*- and *cis*-PB, the quoted numbers are 0.68 and 0.7. With increasing chain length, the ratios diminished gradually. The ratios found by Kröger *et al.* are consistent with the tendency in our f-values (PE:1, PEO:0.81, PEP:0.88, PB:0.9, and PI:0.5) toward values less than one. However, they deviate more from one than other values for f, in particular for PE.

The third observation regards the ratio between the rheological step-length d_{rheo} and the lateral tube size R_e. For all investigated polymers, this ratio lies between 0.6 and 0.8, again significantly larger than the rheological confinement length. Thus, in all dimensions, the microscopic confinement appears to be looser than that concluded from measurements of the dynamic modulus.

Comparing the results from the simple De Gennes approximation (d_{DG}) with the more sophisticated evaluation within the NG-approach, we observe that the effective tube diameter according to d_{eff} from our analysis is close to d_{DG} within 1 . . . 2 Å, however, with larger deviations and variations for PI.

Furthermore, we like to classify our microscopic results in terms of the much considered packing model.[46] The packing model

TABLE VI. Extracted length scales ("tube diameters") from the fit-parameters in Table III.

Polymer	d_{rheo} (Å)	d_{DG} (Å)	R_e (Å)	d_{NSE} (Å)	d_{eff} (Å)	d_{rheo}/d_{NSE}
PE190	31.1	48.8	48.7 ± 0.1	48.7 ± 0.1	48.7 ± 0.1	0.64
PE190-alpha0	31.1	48.8	49.8 ± 0.2	49.8 ± 0.2	49.8 ± 0.2	0.62
PE190-alpha0-f	31.1	48.8	49.8 ± 1.4	49.5 ± 0.9	49.7 ± 1.1	0.63
PEO190	34.5	47.6	48.5 ± 0.2	48.5 ± 0.2	48.5 ± 0.2	0.71
PEO190-alpha0	34.5	47.6	49.5 ± 0.3	49.5 ± 0.3	49.5 ± 0.3	0.70
PEO190-alpha0-f	34.5	47.6	47.8 ± 3.0	59.3 ± 2.5	51.9 ± 2.6	0.58
PEP200	43.3	60.3	57.2 ± 0.2	57.2 ± 0.2	57.2 ± 0.2	0.76
PEP200-alpha0	43.3	60.3	59.8 ± 0.6	59.8 ± 0.6	59.8 ± 0.6	0.72
PEP200-alpha0-f	43.3	60.3	57.4 ± 2.2	65.1 ± 1.4	60.1 ± 1.7	0.67
PB45	40.0	52.2	48.4 ± 0.3	48.4 ± 0.3	48.4 ± 0.3	0.83
PB45-alpha0	40.0	52.2	50.8 ± 0.5	50.8 ± 0.5	50.8 ± 0.5	0.79
PB45-alpha0-f	40.0	52.2	49.5 ± 2.9	55.2 ± 1.9	51.5 ± 2.4	0.72
PI350	60.0	77.0	64.5 ± 0.2	64.5 ± 0.2	64.5 ± 0.2	0.93
PI350-alpha0	60.0	77.0	73.0 ± 0.6	73.0 ± 0.6	73.0 ± 0.6	0.82
PI350-alpha0-f	60.0	77.0	62.0 ± 2.4	122.7 ± 2.8	87.1 ± 2.2	0.49
PI350-alpha0:3	60.0	77.0	79.9 ± 0.5	79.9 ± 0.5	79.9 ± 0.5	0.75
PI350-alpha0:3-f	60.0	77.0	61.3 ± 2.1	150.2 ± 3.5	100.1 ± 2.4	0.40
PI350-alpha0:3-w	60.0	77.0	77.2 ± 0.6	77.2 ± 0.6	77.2 ± 0.6	0.78

connects polymer conformational data with dynamical properties such as the plateau modulus or the entanglement density. It unites the volume filling and conformational characteristics of a polymer into a single chain length independent parameter. Witten *et al.*[48] defined the packing length as the ratio of the occupied volume of a chain, $V_c = M/(\rho N_A)$ (with M = mass of chain, ρ = chain bulk density, and N_A being the Avogadro number) and the unperturbed chain dimension, which takes the form of the mean-square end-to-end distance $\langle R_e^2 \rangle$,

$$p \equiv \frac{M}{\langle R_e^2 \rangle \rho N_A} = \frac{M_0}{\rho N_A l_{seg}^2}. \tag{22}$$

Its rational may be understood from the following considerations: Let us consider the ratio of the volumes, presented by a cube that is spanned by the end to end distance of a chain with mass M: $V = \left(M l_{seg}^2/M_0\right)^{\frac{3}{2}}$ and the space filling volume of this chain $V_c = M/(\rho N_A)$. This ratio presents the number of chains N_{chain} in that volume $N_{chain} = N^{1/2}\left(l_{seg}^3 \rho N_A/M_0\right)$. Solving for $M_e = M_0 N_e$ and inserting p, we have: $M_e = N_{chain}^2 \rho N_A p^3$. With this relation, the plateau modulus assumes the form $G_e \cong \rho k_B T/M_e = k_B T/(N_{chain}^2 p^3)$. Fetters *et al.* have shown that, for $N_{chain} \cong 20$, this relation is universal and is followed basically by all polymers. Following Fetters listings[46] in Table VII, we include the packing length and $N_{chain} = \sqrt{M_e/(\rho N_A p^3)}$ (M_e is taken from rheology), and compare them with our results for the microscopic entanglement volume $V_{micr} = d_{eff}^3 = N_{chain}^3 p^3 \rightarrow N_{chain} = d_{eff}/p$.

d_{eff} was taken as the average of the results obtained by the different fitting variants. The essence of the packing model is that, in order to form an entanglement, a number of N_{chain} different chains have pervade the entanglement volume. Already from the in-trend larger values of d_{eff} from the microscopic observation compared to those derived from rheology, it is clear that the microscopically determined chain confinement appears to be looser than that derived from rheology. Taking into account the packing model, we observe that for all investigated polymers, consistently, the number of chains pervading the entanglement volume is required to be about 40% larger compared to the rheologically derived number.

E. Summary

Summarizing the outcome for the different polymers we point out that as a common result, the effective confinement length or tube diameter d_{eff} is stable within 10% among the fitted model variants (except for PI). Close inspection of the fitting in detail, see e.g., Fig. 6, also supports the conclusion that non-Gaussianity effects influence the Rouse dynamics; thus, the related tube diameters are more accurate. For PE, the difference is marginal while for the other polymers, including NG-effects yields slightly larger d_{eff} values. Thus, the microscopic observation by NSE reliably delivers the microscopic confinement volume $V_{conf} = d_{eff}^3$, which is established by the topological constraints within an estimated confidence range of about 5%–10% (except PI).

TABLE VII. Relation of the tube sizes from Table VI to the packing lengths.

Polymer	p (Å)	N_{chain}^{rheo} (Fetters)	$N_{chain}^{micr} = d_{eff}/p$	$N_{chain}^{rheo}/N_{chain}^{micr}$
PE190	1.75	19.6	28.4	0.69
PEO190	1.94	18.6	25.8	0.72
PEP200	2.52	16.9	23.4	0.72
PB45	2.29	16.9	21.9	0.77
PI350	3.2	18.2	25.1	0.73

Furthermore, it is interesting to note that generally d_{eff} is significantly larger than d_{rheo}, an observation that was already made by the more simple evaluations in terms of Eq. (2).

Finally, a comparison of all available polymer data strongly supports a universal scaling behavior if Q is scaled according to the relevant length scale, namely the tube diameter and the time is scaled by the "blob" relaxation time τ_e rather than by the Rouse rates alone!

VI. S(Q, t) PARAMETRIZATIONS AS A TECHNICAL TOOL

The various semi-empirical approaches combining the ideas of De Gennes, entanglement blob size, and the non-Gaussianity ansatz of Guenza shed some light on the underlying processes leading to the microscopic chain relaxation in long polymer melts and the differences between some polymers. Using previous knowledge on polymer parameters restricts the remaining freedom and still leads to a reasonable description for most of the polymers. This corroborates that the semi empirical models grasp the general scenario on the molecular scale quite well. Thus, all approaches grasp the general shape $S(Q,t)$ with a few parameters, i.e., the underlying mathematical structure is appropriate and allows safe interpolation of $S(Q,t)$ within (and possibly somewhat beyond) the experimentally covered (Q,t)-range.

However, there are still a few imperfections in the data representation. Thus, if just a very good interpolation is needed (e.g., to compare curves obtained at different Q-values within a common range), further parameters may be relaxed in the fitting process leading to a better match. Indeed, this would allow a perfect match of all available data. The deviation of parameters from their expected "physical" values in those cases may be an indication of deficiencies/limitation in our model. In particular, even the PI350K data may be nicely described in this way.

This more technical approach also yields a tool to computationally incorporate the corresponding accurate (long chain) scattering functions in other evaluation schemes as, e.g., the application of RPA corrections in mixtures of (labeled) small chains in a long chain melt as in Refs. 40 and 50.

Finally, we remark that another more recent approach to concisely describe scattering functions of reptation polymers was given by Ma *et al.*;[51] in the supplementary material, we explore its application to the here presented data.

VII. MAIN RESULTS AND CONCLUSIONS

In this work, we have compared the dynamic structure factors for five different polymer melts comprising simple polyolefins (PE and PEP), poly-dienes (PB and PI), and a polyether (PEO). For this purpose, we have further developed the De Gennes approximation for the dynamic structure factor for local reptation. We incorporated approximately the Rouse motion within the topological tube confinement by a Rouse blob of size $R_e = f\, l_{\mathrm{seg}}\sqrt{N_e}$. Tweaking the default value of f away from 1 was used as a tentative path to detect possible tube anisotropies. Using a product ansatz approximation, we described the single chain dynamic structure factor in multiplying the coherent scattering functions for local reptation and Rouse motion within the Rouse blob, which corresponds to a convolution of the corresponding pair correlation functions. For completeness contour length fluctuations (CLFs), Eq. (5) was also integrated to account for some minor CLF-influence on the not very long chains (PB).

The following results stand out:

The simple De Gennes approximation in its exponentiated form is generally used to analyze scattering but also simulation data describes the dynamic structure factor for $t > \tau_e$ reasonably and for several polymers astonishingly well, even though in some cases the predicted functional form does not agree with the spectral data, in particular at short times. It also proves to be problematic to estimate the Rouse rate from the initial decay of long chain melt spectra; here, it is essential to resort to other sources and verify and/or determine it independently from short chain Rouse spectra and/or rheology. In our work, we have decided to fit the Rouse rates Wl^4 with the result that the obtained values are systematically smaller than those obtained from fits of the initial decay of $S(Q,t)/S(Q)$.

Generally, the results for the "De Gennes tube diameters" are within 5% (except PI) of the outcome of the more sophisticated treatments.

Using a convolution approach together with the fully integrated De Gennes structure factor, where the initial relaxation is described as a Rouse relaxation within the confining volume, allows a good description of the entire structure factor for most of the polymers.

As realized by simulations and also for tracer diffusion in highly entangled melts, for all polymers, non-Gaussian dynamics appears to be a valid phenomenon that affects the chain dynamics within the tube. Its consideration improves the quality of the fits.

Comparing with rheology, we confirm that in all cases, the microscopic tube step-length d_{NSE} is significantly larger than the rheological d_{rheo}. Looking at the asymmetry, then we find indications that for all polymers, the tube confinement is found to be leaner compared to the step-length. It is interesting to note that by simulations on PE and PB, the Kröger group found qualitatively similar ratios between step-length and tube diameters as our experiment analysis.[49]

All considered polymer spectra within the NSE time and length scales are generic and scale with each other with scaling factors that match the ratios of d_{eff}-values for Q and Wl^4/d_{eff}^4 for t i.e., have a time scaling according to the "blob" τ_e-ratio.

Finally, in terms of the packing model, we observe that for all investigated polymers consistently the number of chains pervading the entanglement volume is required to be about 40% larger compared to the rheologically derived number.

Software modules to compute the model functions $S(Q,t)$ used in this paper are provided as subroutines in *Fortran* and *C* and are contained in the supplementary material.

SUPPLEMENTARY MATERIAL

The supplementary material contains (i) a description of the modeling consideration and the relation to scattering functions; (ii) a test of other approaches to describe the scattering function of reptating polymers in simple terms; (iii) details of the chemical synthesis of PI350; (iv) detailed consideration to the Rouse rate (Wl^4) determination for various polymers; (v) listing of the software module to compute $S(Q,t)$; and finally (vi) NSE scattering data that were used.

ACKNOWLEDGMENTS

We acknowledge Jürgen Allgaier for the synthesis of polyisoprene PI350 and Stefano Pasini and Peter Falus for the PI measurements. The ILL is gratefully acknowledged for granting the beamtime for the NSE measurements (experiment TEST-2745[52]).

AUTHOR DECLARATIONS

Conflict of Interest

The authors have no conflicts to disclose.

Author Contributions

Michael Monkenbusch: Conceptualization (supporting); Formal analysis (equal); Methodology (lead); Software (lead); Validation (equal); Writing – review & editing (equal). **Martina Kruteva**: Data curation (lead); Investigation (equal); Methodology (supporting); Validation (supporting); Writing – review & editing (equal). **Dieter Richter**: Conceptualization (lead); Formal analysis (equal); Investigation (equal); Methodology (equal); Validation (equal); Writing – original draft (lead); Writing – review & editing (equal).

DATA AVAILABILITY

The underlying NSE data are contained in the supplementary material.

REFERENCES

[1] P. G. de Gennes, "Reptation of a polymer chain in the presence of fixed obstacles," J. Chem. Phys. **55**(2), 572–579 (1971).
[2] M. Doi and S. F. Edwards, "Dynamics of concentrated polymer systems. Part 2—Molecular motion under flow," J. Chem. Soc., Faraday Trans. 2 **74**, 1802–1817 (1978).
[3] M. Doi and S. F. Edwards, *The Theory of Polymer Dynamics* (Clarendon Press, Oxford, 1986).
[4] P. G. De Gennes, *Scaling Concepts in Polymer Physics* (Cornell University Press, Ithaca and London, 1979).
[5] T. C. B. McLeish, "Tube theory of entangled polymer dynamics," Adv. Phys. **51**(6), 1379–1527 (2002).
[6] K. Kremer and G. S. Grest, "Dynamics of entangled linear polymer melts: A molecular-dynamics simulation," J. Chem. Phys. **92**, 5057–5086 (1990).
[7] H.-P. Hsu and K. Kremer, "Detailed analysis of Rouse mode and dynamic scattering function of highly entangled polymer melts in equilibrium," Eur. Phys. J.: Spec. Top. **226**, 693–703 (2017).
[8] A. E. Likhtman, "Single-chain slip-link model of entangled polymers: Simultaneous description of neutron spin-echo, rheology, and diffusion," Macromolecules **38**, 6128–6139 (2005).
[9] M. Rubinstein and R. H. Colby, *Polymer Physics* (Oxford University Press, 2003).
[10] P. E. Rouse, "Theory of the linear viscoelastic properties of dilute solutions of coiling polymers," J. Chem. Phys. **21**(7), 1272 (2004).
[11] K. S. Schweizer, "Mode-coupling theory of the dynamics of polymer liquids: Qualitative predictions for flexible chain and ring melts," J. Chem. Phys. **91**(9), 5822 (1989).
[12] K. S. Schweizer and J. G. Curro, "Integral-equation theory of the structure of polymer melts," Phys. Rev. Lett. **58**, 246 (1987).
[13] J. G. Curro, K. S. Schweizer, G. S. Grest, and K. Kremer, "A comparison between integral equation theory and molecular dynamics simulations of dense, flexible polymer liquids," J. Chem. Phys. **91**, 1357 (1989).
[14] G. Szamel and K. S. Schweizer, "Reptation as a dynamic mean-field theory: Self and tracer diffusion in a simple model of rodlike polymers," J. Chem. Phys. **100**, 3127 (1994).
[15] K. S. Schweizer and G. Szamel, "Crossover to entangled dynamics in polymer solutions and melts," J. Chem. Phys. **103**, 1934 (1995).
[16] K. S. Schweizer, M. Fuchs, G. Szamel, M. Guenza, and H. Tang, "Polymer-mode-coupling theory of the slow dynamics of entangled macromolecular fluids," Macromol. Theory Simul. **6**(6), 1037 (1997).
[17] D. M. Sussman and K. S. Schweizer, "Microscopic theory of entangled polymer melt dynamics: Flexible chains as primitive-path random walks and supercoarse grained needles," Phys. Rev. Lett. **109**, 168306 (2012).
[18] M. Guenza, "Many chain correlated dynamics in polymer fluids," J. Chem. Phys. **110**(15), 7574–7588 (1999).
[19] M. Guenza, "Cooperative dynamics in unentangled polymer fluids," Phys. Rev. Lett. **88**(2), 025901 (2001).
[20] M. G. Guenza, "Theoretical models for bridging timescales in polymer dynamics," J. Phys.: Condens. Matter **20**(3), 033101 (2008).
[21] M. G. Guenza, "Localization of chain dynamics in entangled polymer melts," Phys. Rev. E **89**(5), 052603 (2014).
[22] D. S. Pearson, G. Ver Strate, E. von Meerwall, and F. C. Schilling, Macromolecules **20**, 1133–1141 (1987).
[23] B. Farago, P. Falus, I. Hoffmann, M. Gradzielski, F. Thomas, and C. Gomez, "The IN15 upgrade," Neutron News **26**(3), 15 (2015).
[24] S. Pasini, O. Holderer, T. Kozielewski, D. Richter, and M. Monkenbusch, "J-NSE-Phoenix, a neutron spin-echo spectrometer with optimized superconducting precession coils at the MLZ in Garching," Rev. Sci. Instrum. **90**(4), 043107 (2019).
[25] D. Richter, B. Farago, L. J. Fetters, J. S. Huang, B. Ewen, and C. Lartigue, "Direct microscopic observation of the entanglement distance in a polymer melt," Phys. Rev. Lett. **64**(12), 1389–1392 (1990).
[26] R. Butera, L. J. Fetters, J. S. Huang, D. Richter, W. Pyckhout-Hintzen, A. Zirkel, B. Farago, and B. Ewen, "Microscopic and macroscopic evaluation of fundamental facets of the entanglement concept," Phys. Rev. Lett. **66**(16), 2088–2091 (1991).
[27] D. Richter, R. Butera, L. J. Fetters, J. S. Huang, B. Farago, and B. Ewen, "Entanglement constraints in polymer melts. A neutron spin echo study," Macromolecules **25**(23), 6156–6164 (1992).
[28] D. Richter, B. Farago, R. Butera, L. J. Fetters, J. S. Huang, and B. Ewen, "On the origins of entanglement constraints," Macromolecules **26**(4), 795–804 (1993).
[29] P. Schleger, B. Farago, C. Lartigue, A. Kollmar, and D. Richter, "Clear evidence of reptation in polyethylene from neutron spin-echo spectroscopy," Phys. Rev. Lett. **81**(1), 124–127 (1998).
[30] K. Kremer, G. S. Grest, and I. Carmesin, "Crossover from Rouse to reptation dynamics: A molecular-dynamics simulation," Phys. Rev. Lett. **61**(5), 566–569 (1988).
[31] A. Wischnewski, M. Monkenbusch, L. Willner, D. Richter, and G. Kali, "Direct observation of the transition from free to constrained single-segment motion in entangled polymer melts," Phys. Rev. Lett. **90**(5), 058302 (2003).
[32] M. Kruteva, M. Monkenbusch, J. Allgaier, O. Holderer, S. Pasini, I. Hoffmann, and D. Richter, "Self-similar dynamics of large polymer rings: A neutron spin echo study," Phys. Rev. Lett. **125**(23), 238004 (2020).
[33] P. G. De Gennes, "Coherent scattering by one reptating chain," J. Phys. Paris **42**(5), 735–740 (1981).
[34] H.-P. Hsu and K. Kremer, "Static and dynamic properties of large polymer melts in equilibrium," J. Chem. Phys. **144**, 154907 (2016).
[35] G. Zhang, L. A. Moreira, T. Stuehn, K. C. Daoulas, and K. Kremer, "Equilibration of high molecular weight polymer melts: A hierarchical strategy," ACS Macro Lett. **3**, 198 (2014).
[36] L. A. Moreira, G. Zhang, F. Müller, T. Stuehn, and K. Kremer, "Direct equilibration and characterization of polymer melts for computer simulations," Macromol. Theory Simul. **24**, 419 (2015).
[37] T. Vettorel, G. Besold, and K. Kremer, "Fluctuating soft-sphere approach to coarse-graining of polymer models," Soft Matter **6**, 2282–2292 (2010).
[38] M. Pütz, K. Kremer, and G. S. Grest, "What is the entanglement length in a polymer melt?," Europhys. Lett. **49**, 735–741 (2000).

[39]D. Richter, M. Monkenbusch, A. Arbe, and J. Colmenero, "Neutron spin-echo in polymer systems," Adv. Polym. Sci. **174**, 1–221 (2005).
[40]M. Zamponi, M. Kruteva, M. Monkenbusch, L. Willner, A. Wischnewski, I. Hoffmann, and D. Richter, "Cooperative chain dynamics of tracer chains in highly entangled polyethylene melts," Phys. Rev. Lett. **126**, 187801 (2021).
[41]M. Zamponi, M. Monkenbusch, L. Willner, A. Wischnewski, B. Farago, and D. Richter, "Contour length fluctuations in polymer melts: A direct molecular proof," Europhys. Lett. **72**(6), 1039–1044 (2005).
[42]A. Wischnewski, M. Monkenbusch, L. Willner, D. Richter, A. E. Likhtman, T. C. B. McLeish, and B. Farago, "Molecular observation of contour-length fluctuations limiting topological confinement in polymer melts," Phys. Rev. Lett. **88**, 058301 (2002).
[43]N. Clarke and T. C. B. Mcleish, "The dynamic structure factor of a star polymer in a concentrated solution," Macromolecules **26**(19), 5264–5266 (1993).
[44]B. J. Gold, W. Pyckhout-Hintzen, A. Wischnewski, A. Radulescu, M. Monkenbusch, J. Allgaier, I. Hoffmann, D. Parisi, D. Vlassopoulos, and D. Richter, "Direct assessment of tube dilation in entangled polymers," Phys. Rev. Lett. **122**, 088001 (2019).
[45]D. Salatto, J.-M. Y. Carrillo, M. K. Endoh, T. Taniguchi, B. M. Yavitt, T. Masui, H. Kishimoto, M. Tyagi, A. E. Ribbe, V. Garcia Sakai, M. Kruteva, B. G. Sumpter, B. Farago, D. Richter, M. Nagao, and T. Koga, "Structural and dynamical roles of bound polymer chains in rubber reinforcement," Macromolecules **54**(23), 11032–11046 (2021).
[46]L. J. Fetters, D. J. Lohse, D. Richter, T. A. Witten, and A. Zirkel, "Connection between polymer molecular weight, density, chain dimensions, and melt viscoelastic properties," Macromolecules **27**(17), 4639–4647 (1994).
[47]M. Kruteva, M. Zamponi, I. Hoffmann, J. Allgaier, M. Monkenbusch, and D. Richter, "Non-Gaussian and cooperative dynamics of entanglement strands in polymer melts," Macromolecules **54**(24), 11384–11391 (2021).
[48]T. A. Witten, S. T. Milner, and Z.-G. Wang, in *Multiphase Macromolecular Systems*, edited by B. M. Culbertson (Plenum, New York, 1989).
[49]P. S. Stephanou, C. Baig, G. Tsolou, V. G. Mavrantzas, and M. Kröger, "Quantifying chain reptation in entangled polymer melts: Topological and dynamical mapping of atomistic simulation results onto the tube model," J. Chem. Phys. **132**(12), 124904 (2010).
[50]M. Monkenbusch, M. Kruteva, M. Zamponi, L. Willner, I. Hoffman, B. Farago, and D. Richter, "A practical method to account for random phase approximation effects on the dynamic scattering of multi-component polymer systems," J. Chem. Phys. **152**(5), 054901 (2020).
[51]J. Ma, J.-M. Y. Carrillo, C. Do, W. R. Chen, P. Falus, Z. Shen, K. Hong, B. G. Sumpter, and Y. Wang, "Spatial correlations of entangled polymer dynamics," Phys. Rev. E **104**, 024503 (2021).
[52]M. Kruteva, P. Falus, and D. Richter, Influence of Polymer-Surface Interaction on Entangled Dynamics, Institut Laue-Langevin (ILL), 2017.